Journal of Membrane Science 385–386 (2011) 10–19

Contents lists available at ScienceDirect

Journal of Membrane Science

journal homepage: www.elsevier.com/locate/memsci

Electrospun nanofiber supported thin film composite membranes for engineered osmosis

Nhu-Ngoc Bui[a], Mary Laura Lind[b,c], Eric M.V. Hoek[b], Jeffrey R. McCutcheon[a,*]

[a] Department of Chemical, Materials & Biomolecular Engineering and Center for Environmental Sciences and Engineering, University of Connecticut, Storrs, CT, USA
[b] Department of Civil & Environmental Engineering and California NanoSystems Institute, University of California, Los Angeles, Los Angeles, CA, USA
[c] School for Engineering of Matter, Transport and Energy, Arizona State University, Tempe, AZ, USA

ARTICLE INFO

Article history:
Received 25 April 2011
Received in revised form 20 July 2011
Accepted 2 August 2011
Available online 9 August 2011

Keywords:
Forward osmosis
Pressure retarded osmosis
Composite membrane
Electrospinning
Nanofiber
Polyamide
Polysulfone
Polyethersulfone

ABSTRACT

Engineered osmosis (EO) is a membrane based separation technology with applications to sustainable energy, resource recovery, and water production. Still emerging, EO utilizes energy stored as chemical potential (osmotic pressure) to generate power or purify water, but the lack of membranes with suitable water flux, solute rejection, mechanical strength, and chemical stability has limited EO development. In this study, we attempt to address low water flux by proposing a novel thin film composite membrane for EO. This TFC membrane comprises an electrospun polymeric nanofiber support layer and a polyamide skin layer formed by *in situ* polymerization. The best nanofiber supported-polyamide composite membranes exhibited two to five times higher flux with up to 100 times lower salt flux than a standard commercial forward osmosis membrane. These results suggest that electrospun nanofiber supported polyamide composite membranes may enable applications like forward osmosis where internal concentration polarization is the performance-limiting factor. More research is needed to establish the applicability of this new membrane design for engineered osmosis applications involving harsh chemical environments and elevated mechanical pressures.

© 2011 Elsevier B.V. All rights reserved.

1. Introduction

Overcoming global scarcity of water, energy, and other natural resources (e.g., nutrients, metals, minerals, etc.) are grand challenges faced by humanity today. These critical resources are inextricably linked, and therefore, must be considered together as new technologies are developed. Engineered osmosis™ (EO) is a unique and emerging platform technology that may ultimately help address water, resource, and energy scarcity by enabling the harvesting of salinity gradients for electricity generation (pressure retarded osmosis, PRO), concentrating high-value dissolved solids for recovery and beneficial reuse (direct osmotic concentration, DOC), and converting saline waters to fresh water (forward osmosis, FO) [1–4]. Hence, there is great interest in EO because it offers the potential to enable a wide range of new, sustainable processes through a single platform technology.

EO technologies harness osmotic potential energy to drive water across a membrane from a dilute feed solution into a concentrated draw solution. These emerging osmotic pressure driven processes demand redesign of semi-permeable membranes, most of which, such as those for reverse osmosis (RO), were designed for hydraulic pressure driven operation. Traditional RO and nanofiltration (NF) membranes employ an ultra-thin selective barrier layer supported by multiple robust, porous polymer support layers. A common RO membrane design comprises an aromatic polyamide thin film coated onto an integrally skinned asymmetric polysulfone or polyethersulfone membrane cast by phase inversion over a polyester nonwoven fabric [5]. This thin film composite (TFC) membrane design serves as the basis for most commercial NF and RO membranes.

The excellent performance of TFC membranes in the early 1970s led to exhaustive development of the composite structure where each layer was independently tailored to produce optimal performing membranes for a range of separations [6–8]. For traditional RO membranes, the layer of greatest importance is the selective layer since it is this layer that primarily determines the membrane permselectivity, while the support layers primarily serve to provide mechanical support for the membrane during fabrication, handling, and operation. Therefore, much effort has been focused on improving the properties of the selective layer (permselectivity and longevity) [9–22], while the support layer has been relatively ignored.

However, in EO the support layer plays a crucial role in membrane performance. The osmotic driving force is established solely across the membrane selective layer. The downstream interface

* Corresponding author at: University of Connecticut, 191 Auditorium Rd., Unit 3222, Storrs, CT 06269-3222, USA. Tel.: +1 860 486 4601; fax: +1 860 486 2859.
E-mail address: jeff@engr.uconn.edu (J.R. McCutcheon).

0376-7388/$ – see front matter © 2011 Elsevier B.V. All rights reserved.
doi:10.1016/j.memsci.2011.08.002

of this layer is embedded within the support layer. During osmosis, solutes must diffuse through the support layer to or from this internal interface. The thick, low porosity support materials commonly used in RO membrane supports create resistance to solute mass transfer and result in a boundary layer phenomenon known as *internal concentration polarization* (ICP). As such, RO membranes, which were never intended for this type of use, have performed poorly in EO performance tests in previous investigations [1–3,23–25].

It has been shown that ICP is a prominent factor of poor flux performance in osmosis-driven membrane processes [26–28]. Unlike traditional CP, referred to as external concentration polarization (ECP) in this study, the influence of ICP on inhibiting the permeate flow cannot be mitigated by altering hydrodynamic conditions as it is protected by the confines of the support structure. ICP is primarily influenced by the support layer structure, which reduces the effective solute diffusivity and mass transfer coefficient. Theoretical analysis has led to the establishment of a structure parameter, $S = t\tau/\varepsilon$ (where t, τ and ε are the thickness, tortuosity and porosity, respectively, of the support layer), which defines an effective diffusive path length (or effective thickness) of the support layer [29,30]. Reducing mass transfer resistance requires the reduction of this parameter. New support layers are thus needed that exhibit minimal thickness and tortuosity combined with a high porosity. Its chemistry should also be optimized to obtain suitable intrinsic hydrophilicity, mechanical strength, and chemical stability [22].

Recent achievements in developing high-flux EO membranes have been reported with tubular and flat sheet membranes. Wang et al. have developed novel hollow fiber TFC membranes exhibiting high water flux [31]. Arena et al. modified the supports of commercial RO membranes with polydopamine [32]. Yip et al. developed new flat sheet membranes by tailoring support layers for TFC membranes with mixes of finger-like and sponge-like morphologies [30]. Each of these approaches is promising, having exceeded performance of the commercial standard membrane from Hydration Technologies Innovations (HTI) used in almost all studies on FO in the past decade. However, even these membranes fall far below expected fluxes and much work remains to be done to improve upon the performance of TFC membranes.

This study introduces a novel flat-sheet polyamide composite membrane supported by a nonwoven web of electrospun nanofibers. The fibers were electrospun onto a commercial polyester (PET) nonwoven fabric. The polyamide selective layer was polymerized *in situ* onto the nanofiber support through an interfacial polycondensation reaction commonly used in fabricating RO membranes [5]. We hypothesized that a more porous mid-layer separating the polyamide thin film and the nonwoven fabric novel support membrane should enhance osmotic flux by minimizing ICP.

2. Materials and methods

2.1. Materials

Polyethersulfone (PES, RADEL H-3000, $M_w = 7.8 \times 10^4$ g/mol, $M_n = 2.5 \times 10^4$ g/mol) and polysulfone (PSf, UDEL P-3500, $M_w = 8.0 \times 10^4$–8.6×10^4 g/mol, $M_n = 2.3 \times 10^4$ g/mol) were provided by Solvay Advanced Polymers. Polyester nonwoven fabric (PET, FO 2425N/30) sheet was obtained from Freudenberg (Weinheim, Germany). Commercial asymmetric cellulose triacetate forward osmosis membranes (CA) were provided by Hydration Technology Inc. (HTI, Albany, OR) for comparison. N,N-dimethylformamide (DMF, anhydrous, 99.8%), N-methyl-2-pyrrolidone (NMP, anhydrous, 99.5%), 1,3,5-benzenetricarbonyl trichloride (TMC, 98%), m-phenylenediamine (MPD, >99%), sodium bisulfite ($NaHSO_3$, A.C.S. reagent), sodium hypochlorite (NaOCl, solution, available chlorine 10–15%) were obtained from Sigma–Aldrich. Sodium dodecyl sulfate (SDS, 99%) was provided by Fisher Scientific. Isopar-G, referred to hereafter as "isopar", was purchased from Gallade Chemical. All chemicals were used as received. For the osmotic flux tests, sodium chloride (NaCl, crystalline, certified ACS, Fisher Scientific) and deionized water from a Millipore Integral 10 water system (Millipore, USA) were used.

2.2. Fabrication of nonwoven porous support layers using electrospinning

DMF is a commonly used solvent in preparing polymeric solutions for electrospinning. However, as discussed in previous investigations [33,34], the high vapor pressure of DMF at 25 °C, which is of 3.85 mm Hg, allows it to evaporate quickly during the spinning process. The resulting nanofibers depositing on the PET backing layer may dry between leaving the nozzle and depositing preventing good adhesion to other deposited fibers or to the PET substrate. Poor fiber–fiber adhesion and fiber–substrate adhesion results in a low quality support for interfacial polymerization due to poor mechanical strength and an infirm surface. NMP which has lower vapor pressure of 0.5 mm Hg at 25 °C [34] was mixed with DMF to reduce the solvent evaporation rate [33]. The ratio of DMF and NMP solvents was adjusted in a suitable range to obtain reasonable adhesion between the electrospun nonwoven mid-layer and the PET backing layer and to achieve desirable nanofibers structure. This ratio strongly impacts the morphology of fibers as well as the wetness of the nanofibers support. It is crucial that the fibers deposit onto the PET while still wet enough to enable soldering of the nanofiber junctions and increasing the PSf nanofibers–PET nonwoven adhesion [33,35]. Tang et al. [33] was one of the first to accomplish this for membrane applications while employing a wet "primer layer" before depositing smaller and more uniform nanofibers.

In our approach, homogeneous solutions of 25% (by weight) of PSf and 20% PES in bi-solvent systems of DMF and NMP at various solvent ratios (DMF/NMP = 10/0, 9/1, 8/2, 7/3, 5/5 and 3/7, w/w) were separately prepared by stirring at 60 °C in 8 h and then overnight at room temperature. The as-prepared polymeric solutions were electrospun onto a PET nonwoven scaffold under a high voltage field of 27.5 kV with a distance between the spinneret and the rotating drum collector of 16 cm. The experiments were operated at 25 °C in a 10% RH atmosphere. The flow rate was reduced from 1.2 ml/h to 0.9 ml/h and 0.6 ml/h after fixed time periods.

The PSf support membranes were first immersed in an aqueous solution of 3.4 wt% MPD for 2 min. Excess MPD solution was removed from the support membrane surface using an air knife. The membrane was then dipped into a solution of 0.15 wt% TMC in isopar for 1 min to form an ultrathin polyamide film. The post-treatment steps for the composite membrane included thermally treating with DI water at 95 °C for 2 min, rinsing with 200 ppm NaOCl and 1000 ppm $NaHSO_3$ aqueous solutions at ambient temperature for 2 min and 30 s, respectively, and heat-curing again with DI water at 95 °C for 2 min. The as-prepared TFC polyamide membrane was stored in DI water at 4 °C [36].

2.3. Membrane characterization

Surface morphology and cross-sectional structure of the electrospun supports and the TFC polyamide membranes were qualitatively evaluated with scanning electron microscopy (SEM). A cold cathode field emission scanning electron microscope JSM-6335F and a FEI Phenom desktop SEM (FEI Company, USA) were used for imaging. Before imaging, the samples were kept overnight in a desiccator and then sputter coated with a thin layer of gold

(Au) and platinum (Pt) to obtain better contrast and to avoid charge accumulation. The average diameter of nanofibers was calculated from 50 nanofibers imaged at different spots of the fiber mats using ImageJ software.

A CAM 101 series contact angle goniometer was used to measure the contact angle of the electrospun nonwoven substrates. Attenuated total reflection Fourier-transform infrared (ATR-FTIR) spectroscopy was used to confirm the successful fabrication of the polyamide skin layer on the top of the nonwoven PES/PSf support by the *in situ* interfacial polycondensation process. Spectra were taken in a (FT/IR 670 plus; Jasco, Easton, MD) with a variable angle attenuated total reflection (ATR) attachment coupled to a germanium crystal operated at 45° in an argon environment. Furthermore, focused ion beam (FIB) characterization on the PSf-based TFC polyamide membrane was conducted to observe the interface between the polyamide skin layer and the electrospun support. This analysis was carried out using a FEI Strata 400 STEM Dual-Beam system which combines the Field Emission Scanning Electron Microscope (FE-SEM) with Focused Ion Beam (FIB) technology and Flipstage/STEM assembly. The samples were first sputter coated with a thin layer of Au and Pt. The characterized area of membrane was then locally coated with Pt to dissipate the charges. By scanning the sample with a gallium ion beam, a selected area of polyamide was removed and the interface between PA skin layer and its PSf support was observed.

2.4. Membrane flux performance in direct osmosis (DO) system

Osmotic water flux and reverse salt leakage through electrospun-PSf-based TFC membranes with and without PET support layers were characterized using a custom lab-scale cross-flow forward osmosis system. The experimental setup was described in details elsewhere [3,22]. A 1.5 M sodium chloride solution was used as the draw solution while DI water was used as the feed solution. The hydraulic pressures of the feed and draw solutions were the same (6.9 kPa). Due to differences in fluid density, the observed flow rates of the feed and draw solution were 0.6 and 0.9 liter per minute (LPM), respectively. The temperatures of the feed and draw solutions were maintained at $23 \pm 1\,^{\circ}$C using a recirculating water bath and a heat exchanger. Conductivity of the feed was measured to estimate the reverse salt leakage through the membrane.

Osmotic flux tests were carried out with the membrane oriented in the PRO mode (the membrane active layer faces the draw solution). The system was first run with DI water on both sides of the membrane to stabilize the temperature and purge the air out of the system. Concentrated NaCl (5 M) stock solution was then added into the draw side to establish a desired 1.5 M NaCl solution and the flux was measured. 60 min after the addition of NaCl to the draw solution, an appropriate amount of 100 mM sodium dodecyl sulfate (SDS) aqueous stock solution was added into the feed solution to bring its concentration to 1 mM SDS.

Though the PET nonwoven supports the whole membrane mechanically, it can contribute to mass transfer resistance in EO applications. In one of our previous studies, the PET noticeably contributed to the severe internal concentration polarization [22]. Therefore the PET layer was carefully removed for some tests. A similar approach was taken in our previous investigations [22]. These membranes are referred to PSf^{n}–PET and PSf^{n} samples hereafter. The superscript "n" indicates the electrospun nanofiber support.

The osmotic water flux, J_w, was calculated by dividing the volumetric flux by the membrane area. By measuring the conductivity of the feed solutions at certain time points during the tests, the salt flux, J_s, was calculated by dividing the NaCl mass flow rate by the membrane area. The osmotic water permeability coefficient, A, was determined from the osmotic water flux using:

$$A = \frac{J_w}{\pi_{D,b}\exp(-(J_w/k)) - \pi_{F,b}} \quad (1)$$

where $\pi_{D,b}$ and $\pi_{F,b}$ are the osmotic pressures of the draw and feed solutions in the bulk, respectively. The osmotic pressure of the feed solution in the bulk was derived from the concentration of the feed obtained from conductivity measurements. The mass transfer coefficient, k, was related to Sherwood number for laminar flow in a rectangular channel [3]. In Eq. (1), it was assumed that the osmotic pressures of the draw solution at the membrane surface and in the bulk are linearly proportional to the corresponding concentrations. Also, the ICP effect was not directly accounted for in this study since DI water was used in the feed solution (against the support layer). However, some ICP is expected to occur as a result of salt crossover from the draw solution. Therefore, we also calculated the observed solute permeability coefficient, B, by dividing the salt flux by the bulk concentration difference between draw and feed solutions.

3. Results and discussion

3.1. Characteristics of the polymeric support layers

Fig. 1 shows the different morphologies of the fibers spun from solutions of PSf with various solvent systems. The average diameter of these fibers is about 250 nm. A large number of beads and microspheres appeared in the PSf support derived from solution with 30% DMF in the solvent system with NMP. Beads must be avoided as their presence is indicative of weak, non-uniform fibers [37]. With increased concentration of DMF (70%, 80%, 90% and 100%), the fibers appeared smoother and exhibited fewer beads and defects. However, PSf fiber mats spun from solutions having 80%, 90% or 100% of DMF in the solvent system appeared dry and exhibited poor adhesion to the PET nonwoven fabric. Therefore, we selected a ratio of 70% DMF and 30% NMP for both polysulfone and polyethersulfone fiber mats.

3.2. Characterization of thin film composite membrane

3.2.1. Imaging with scanning electron microscopy

Cross-sectional SEM images in Fig. 2 allow for comparison of the CA membranes obtained from HTI (a and b) and our electrospun fibers supported TFC polyamide membranes (c and d). Fig. 2 shows that the thicknesses of both the support and the active layers in our lab-made TFC are much thinner than those of the commercial cellulose acetate TFC membrane. The cellulose acetate membrane is also imaged in its dried state and is thicker when hydrated. We expect thin nanofiber nonwoven supports with high porosity and low tortuosity to reduce the severity of internal concentration polarization by increasing the mass transfer coefficient in the vicinity of the active layer–support layer interface. Imaging also indicated that the polyamide formed a continuous film on top of the nanofiber support. However, the adhesion was poor between the polyamide and PES nanofibers. Fig. 3 shows that the polyamide layer delaminated from the PES support. In some cases, the polyamide detached and folded back on itself after handling. The PA film exhibited stronger adhesion to the PSf substrate (Fig. 4). In some cases, the PA layer wrapped around the PSf fibers.

We hypothesize that these differences are the result of a specific chemical interaction between the polysulfone or polyethersulfone and the polyamide layers. Water contact angle of electrospun PES is 121 ± 10 and electrospun PSf is $139 \pm 10^{\circ}$. These small differences are likely not enough to fundamentally change the adhesion energy with the polyamide. The chemical difference between PSf and PES is the bisphenol A moiety (Table 1). This moiety may contribute

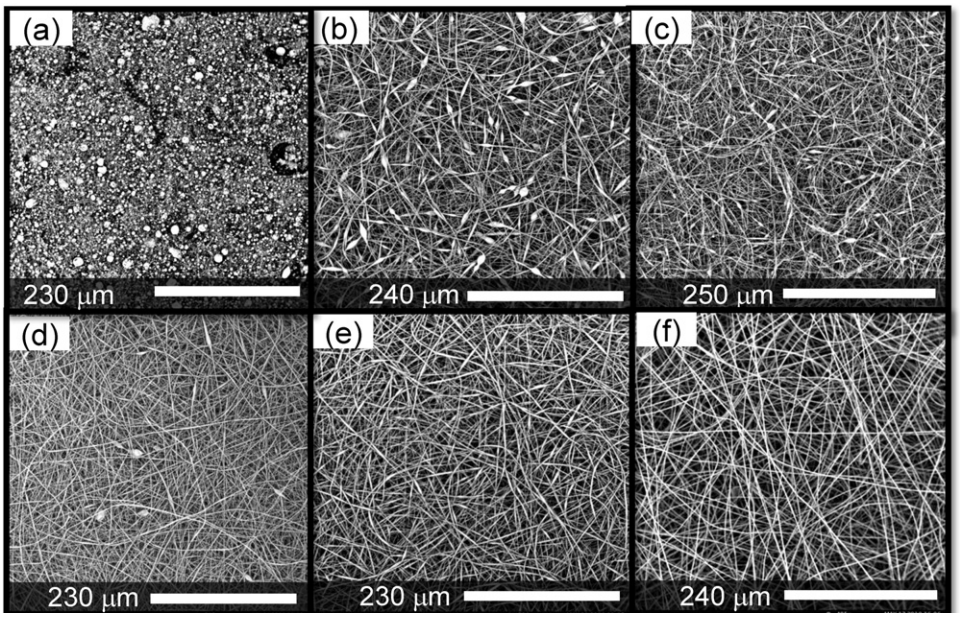

Fig. 1. SEM images for the nanofibrous polysulfone support which were electrospun from 25 wt% PSf solutions at different DMF/NMP ratio of (a) 3/7, (b) 5/5, (c) 7/3, (d) 8/2, (e) 9/1 and (f) 10/0 at magnifications of (a) 510×, (b) 475×, (c) 485×, (d) 505×, (e) 510× and (f) 485×.

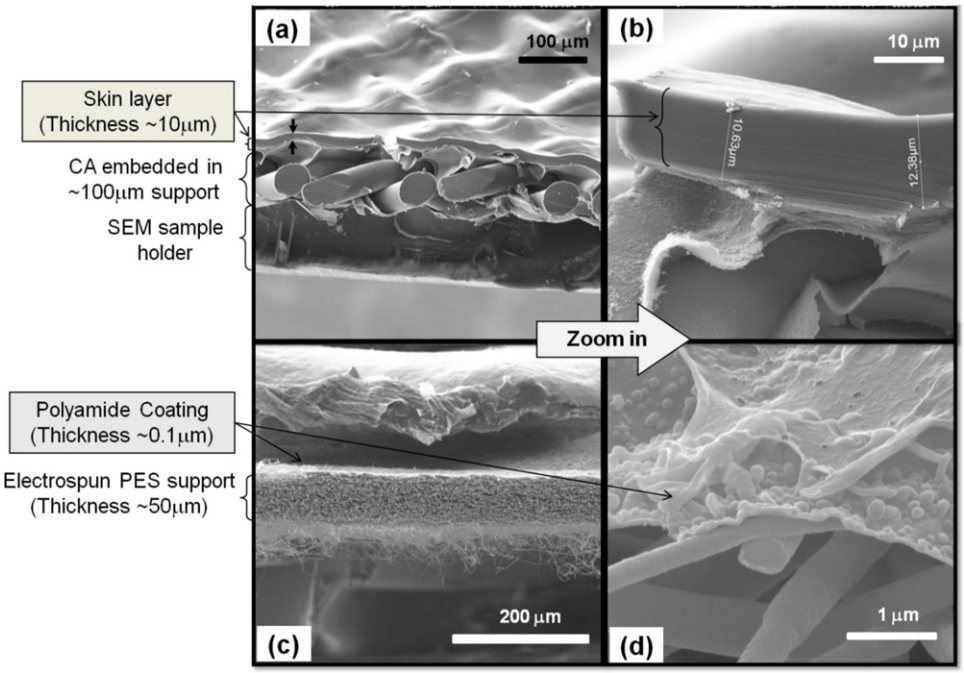

Fig. 2. Cross-sectional SEM images of (a and b) CA commercial membrane and (c and d) TFC electrospun porous support at magnifications of (a) 250×, (b) 2500×, (c) 250× and (d) 32,500×.

Table 1
Molecular structures of polyethersulfone (PES) and polysulfone (PSf).

Polymer	Molecular structure
Polyethersulfone (PES)	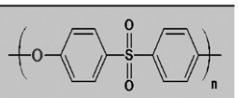
Polysulfone (PSf)	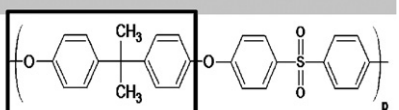

Bisphenol-A

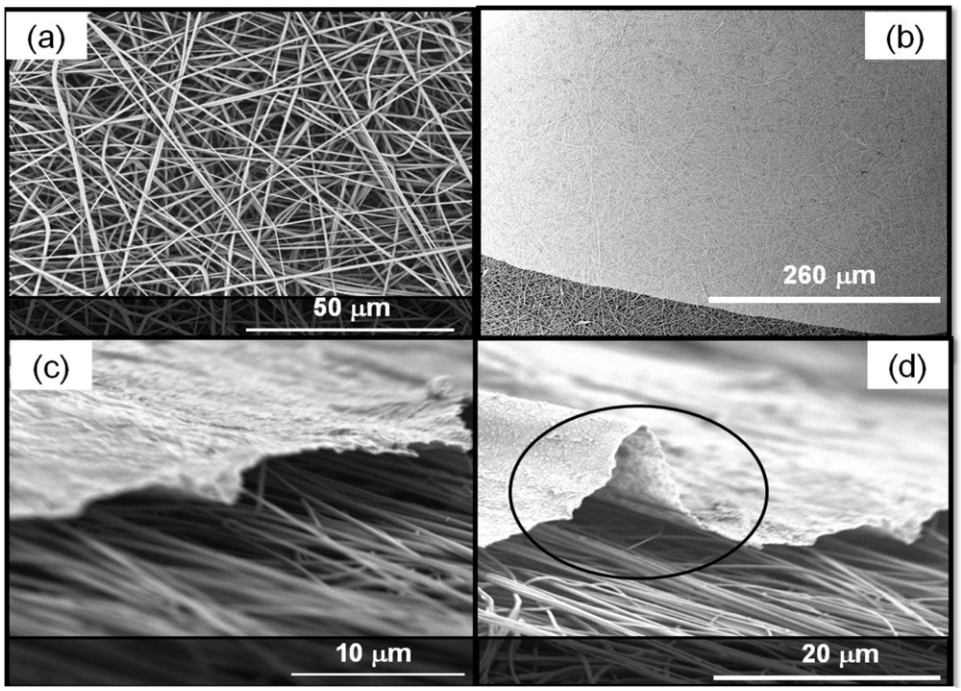

Fig. 3. SEM images of (a) electrospun PES and (b–d) PES-based TFC polyamide membranes at magnifications of (a) 2200×, (b) 460×, (c) 8850× and (d) 5750×. Images (c) and (d) show poor adhesion between polyamide and polyethersulfone nanofiber support.

to the better adhesion between PSf and a polyamide derived from MPD and TMC through a more specific chemical interaction.

While the –COCl functional groups in TMC play an important role in cross-linking with the amine groups in MPD, some of them do not take part into this cross-linking process. These COCl– groups may be, in part, hydrolyzed to form carboxylic acid [7]. The C–Cl bond in the carbonyl groups is very weak due to the polar distribution of electrons in the structure of TMC. Therefore, it tends to be broken to form Cl^- and an electrophile having positively charged carbon site. This electrophile can attract an electron-rich group like –OH to form a carboxylic structure via the hydrolysis mechanism. Also, it may attack the electron-rich aromatic ring in the bisphenol A moiety of polysulfone. The bisphenol A moiety also contains electron rich $–CH_3$ groups. These electrons can be donated to the two aromatic rings, activating them toward electrophilic attack. As a result, the electrophile will replace a hydrogen atom at the *ortho*

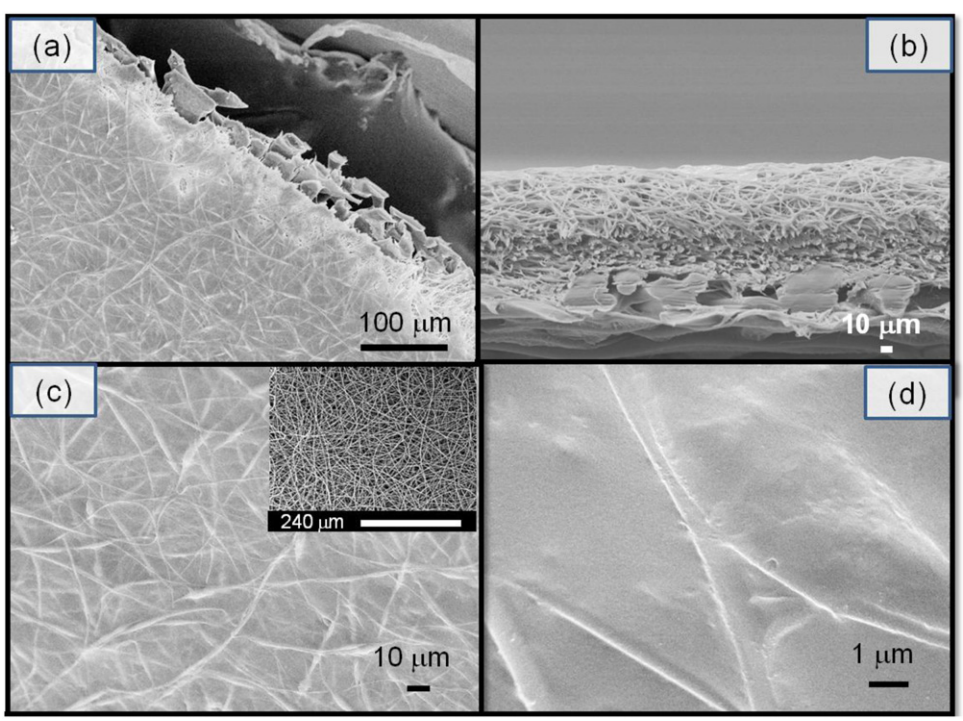

Fig. 4. SEM images of electrospun PSf (insert in c) and PSf-based TFC polyamide membranes at magnifications of (a) 220×, (b) 300×, (c) 600×, (d) 10,000×. Image (b) was viewed from a 90°-angle cross section.

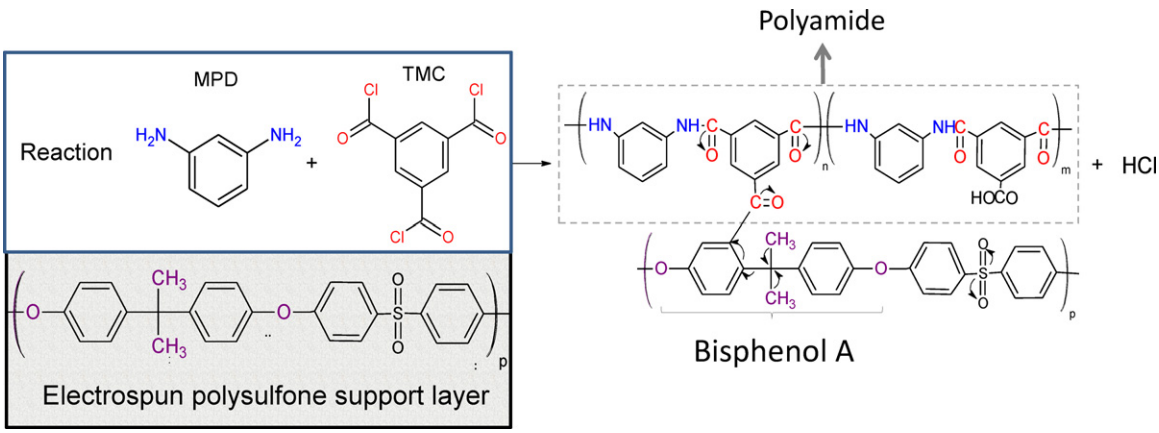

Fig. 5. Diagram of a possible cross-linking interaction between polyamide and the bisphenol A group of polysulfone. Arrows show the proposed reaction mechanism.

site of the aromatic ring via the electrophilic aromatic substitution mechanism or, more specifically, the Friedel–Crafts acylation mechanism [38]. This mechanism can be catalyzed by the presence of hydrochloric acid formed as a by-product of the interfacial polycondensation and the high temperature of about 95 °C used in the post-formation rinses. The hypothesized cross-linking interaction between polyamide skin film and polysulfone substrate has been shown in Fig. 5. It is important to note that the yield of this proposed reaction mechanism need not be high to promote good adhesion, since even a small number of covalent bonds would significantly enhance adhesion over Van der Waals forces.

3.2.2. ATR-FTIR spectroscopy of supports and PA layers

Fig. 6 shows the ATR-FTIR spectra of the fingerprint region of uncoated PES support and PA-coated PES. The IR spectrum of the composite samples is composed of bands attributed to both PA film and PES scaffold. Arrows indicate peaks specific to the composite membrane. Peaks in both support and composite membrane between 1000 and 1400 cm^{-1} are characteristic of the PES support [39]. Most new peaks appearing in the composite membrane are characteristic of the polyamide coating such as peaks at 1661 cm^{-1} (C=O of amide), 1610 cm^{-1} (aromatic ring breathing), and 1544 cm^{-1} (C–N stretch of amide II). Additional peaks at 1450 cm^{-1} and 1734 cm^{-1} are due to the carboxylic acid groups (C–O stretching/O–H bending and C=O stretching) [21,39]. In Fig. 7, the spectrum of the PA-coated membrane supported by PSf has also displayed a strong band at 1650 cm^{-1} (amide I) which is characteristic of C=O band of an amide group. Furthermore, other bands characteristic of PA are also seen at 1610 cm^{-1} and 1540 cm^{-1}. Table 2 demonstrates a summary of probable assignments of IR bands for the PSf/PES–PA composite membrane surface.

3.2.3. Focused ion beam analysis on the PSf-based TFC membrane

An important advantage of using electrospun nanofiber mats as a support for TFC membranes is their high surface porosity. High surface porosity increases the effective active area of the membrane by reducing the amount of the PA layer that is "masked" by the support layer. Fig. 8 shows the PSf nanofiber supported TFC membrane. Removing the polyamide film with a focused ion beam exposed the underlying mesh of nanofibers and their junctions. From the open porous structures of the PSf layer, it can be seen that there is an extremely high surface porosity of the underlying nanofibers. This ensures that a significant amount of the PA layer is exposed to the draw solute during forward osmosis. Fig. 8 also shows the extent to which the polyamide layer forms both on and around the PSf nanofibers. The polyamide layer clearly mirrors the underlying PSf nanofiber morphology underlying it while spanning the gaps between fibers (Fig. 8a and b). In Fig. 8c, the focused ion beam was used to etch away a small area of the polyamide coating film, thus revealing the coating film layer to be less than 1 μm in thickness, probably on the order of 400–500 nm. This further supports improved adhesion between the PA and PSf layers.

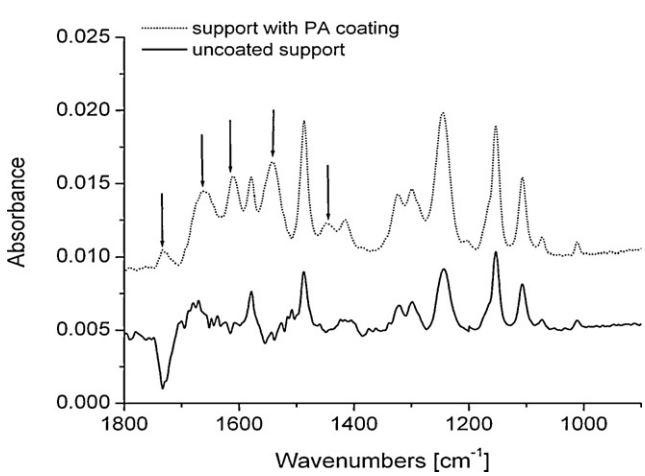

Fig. 6. ATR-IR spectrum of PES nanofiber support (black curve) and PES nanofiber-supported TFC membrane (grey curve).

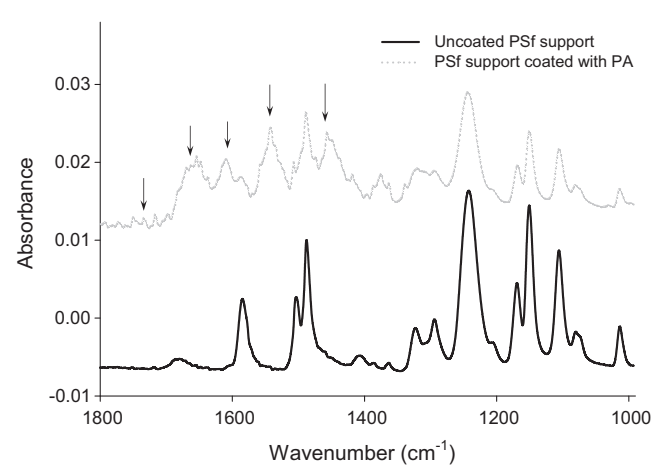

Fig. 7. ATR-IR spectrum of the PSf nanofiber support (black curve) and PSf nanofiber supported TFC membrane (grey curve).

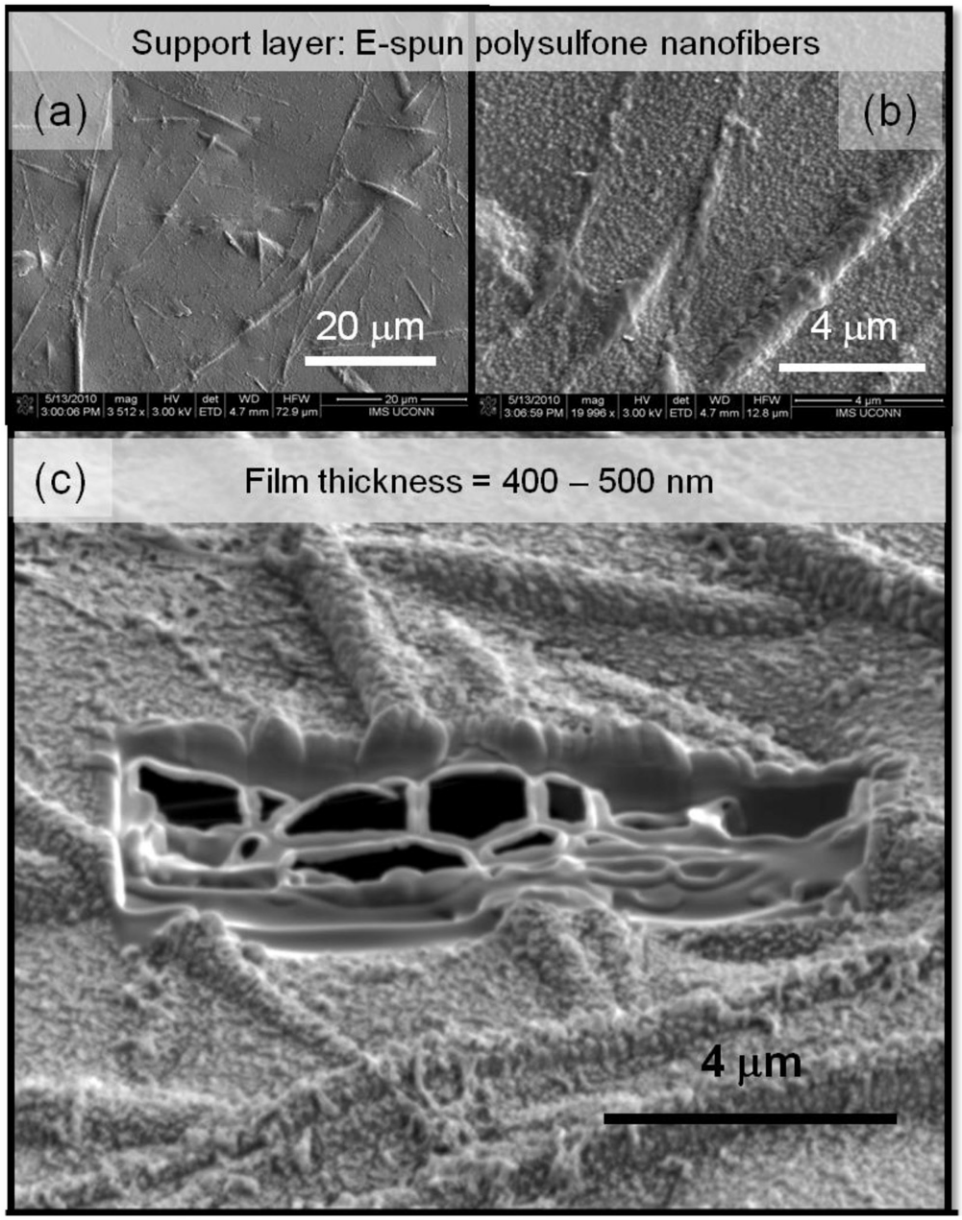

Fig. 8. Focused ion beam (FIB) images of polysulfone-supported thin film composite polyamide membrane at magnifications of (a) 3512× and (b and c) 19,995×.

Table 2
Likely assignments of the IR spectra of the polyethersulfone, polysulfone, and polyamide-coated polyethersulfone/polysulfone composite membranes [21,39,50,51].

Spectra assignment	Frequency (cm^{-1})	Polymers
Skeletal aliphatic C–C/aromatic hydrogen bending/rocking	1072, 1108, 1014, 1080, 1106, 1169	PES, PSf
SO_2 symmetric stretch	1151	PES, PSf
S=O stretching and C–SO_2–C asymmetric stretching	1294, 1325, 1295, 1323	PES, PSf
Aryl-O-aryl C–O stretch	1244	PES, PSf
C=C aromatic ring stretching	1418, 1410	PES, PSf
Characteristic of PES	1486	PES
CH_3–C–CH_3 symmetric deformation	1365, 1385	PSf
CH_3–C–CH_3 stretching	1488	PSf
C=C aromatic ring stretching	1502, 1586	PSf
Carboxylic acid (C–O streching/O–H bending)	1450	PA
C–N stretch (amide II)	1544	PA
Aromatic ring bending	1610	PA
C=O stretching (amide I)	1661	PA
C=O stretching (acid)	1734	PA

Table 3
TFC polyamide membrane separation performance.

		Observed water flux (LMH) @ $\Delta\Pi$ = 76 bar	Observed salt flux (g/m^2 h) @ ΔC = 1.5 mol/l	Water permeability, A (m/kPa s)	Salt permeability, B (m/s)	Figure of merit, $(A^2/B) \times 10^9$ (m/kPa^2 s)
PSf^m–PET	Before adding SDS	26.0	2.26×10^{-3}	1.74×10^{-9}	1.26×10^{-11}	238.60
	After adding SDS	33.6	4.62×10^{-2}	2.68×10^{-9}	3.08×10^{-10}	23.26
PSf^m	Before adding SDS	24.0	8.63	1.59×10^{-9}	4.79×10^{-8}	0.05
	After adding SDS	86.1	36.40	3.02×10^{-8}	1.07×10^{-6}	0.85
CA	No SDS	15.5	1.13×10^{-1}	8.58×10^{-10}	5.23×10^{-10}	1.41

3.3. Osmosis-driven flux

Osmotic flux data for nanofiber-supported polyamide composite membranes are shown in Fig. 9 for PRO mode of operation. The PRO mode was used for these initial experiments to better test the PA layer integrity and to calculate the A and B values without unknown contributions from the support. Membranes with and without a PET layer were evaluated. Initially, both composite membranes exhibited similar fluxes which were about 50% higher than the commercial HTI-CTA membrane. The results are shown in Table 3.

According to McCutcheon and Elimelech [22], the support layer chemistry plays an essential role in osmosis across TFC membranes. The more hydrophobic support materials do not fully wet out in osmosis-driven processes. Since solute transport can only happen through the "wetted porosity" of the support layer, the unsaturated pore structure results in an increased effective structure factor. To determine whether wetting was impacting the flux through our membranes, SDS was added (to a concentration of 1 mM) to the feed solution at 60 min. The SDS reduced the surface tension of the feed solution and facilitated complete wetting of the support layer. Both membranes exhibited increased water flux when SDS was added to the feed. However, the impact of SDS on the PSf^m–PET membrane was far less pronounced and occurred over a longer period of time due to the mass transfer resistance imparted by the PET on SDS diffusion into the PSf nanofibers. The flux for the PSf^m composite membrane after SDS introduction was three to five times higher than the HTI-CA membranes for the same test conditions.

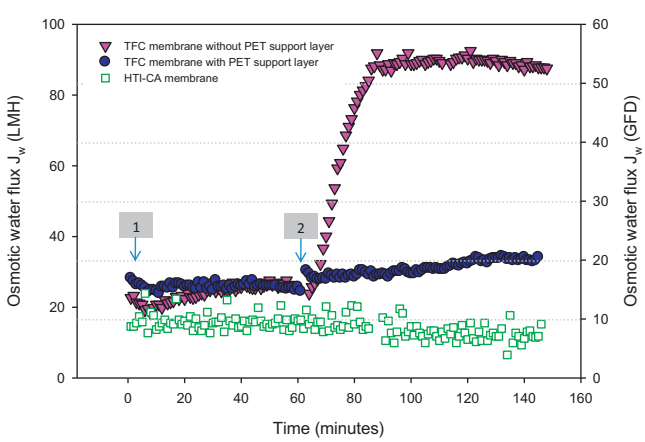

Fig. 9. Water flux through the electrospun PSu-supported TFC polyamide membranes with (circle) and without (triangle) a PET backing layer. Flux performance of the CA membrane (square) under the same test conditions is also shown. Label 1 indicates the start of the test where 5 M NaCl stock solution was added into DI water to achieve a 1.5 M NaCl draw solution. Label 2 (60 min after the start of the test) indicates when SDS was added to the feed side (a final concentration of 1 mM SDS). *Experimental conditions*: membrane oriented in the PRO mode; 1.5 M NaCl draw solution; deionized water feed solution; measured volumetric flow rate of the feed and draw solution were 0.6 and 0.9 LPM, respectively; temperature of both feed and draw solution was 23 ± 1 °C.

These results mirror those found with the use of commercial RO TFC membranes [22].

Table 3 summarizes the performance characteristics of the HTI-CA membrane and the hand-cast nanofiber supported TFC membranes. Performance is represented by the apparent osmotic water, A, and salt, B, permeability coefficients as well as the classical 'figure of merit' A^2/B [24]. Generally, A^2/B decreases with increase of A. The PSf^m membrane produced the highest water permeability (after SDS introduction), but also the highest salt permeability. This membrane may be desirable for EO processes where high flux is critical, but solute rejection is not a primary performance target. The PSf^m–PET membrane produced more than double the flux of the HTI-CTA membrane and the highest figure of merit of 239 μm/MPa^2 s (nearly 200 times that of HTI-CTA). Hence, this membrane may be better suited for EO applications where high flux is more important than selectivity.

The reverse salt flux leaking through the PSf^m–PET membrane (2.3×10^{-3} g/m^2 h) was two orders of magnitude lower than that through the commercial CA membrane (1.3×10^{-1} g/m^2 h). After removal of the PET layer (the PSf^m membrane), the salt flux increased by nearly three orders of magnitude. Removing the PET could result in defects on the PA layer. If this is the case, however, the flux does not change appreciably, suggesting that a decrease of selectivity is countered by a reduction of internal concentration polarization. There was significant increase in salt flux exhibited with both membranes after adding SDS to the feed. Salt fluxes through PSf^m–PET and the PSf^m increased by factors of 20.4 and 4.2, respectively. This could be due to the delamination of the PA from the support after a long exposure to the cross-flow. It may also be due to swelling of the PA film. Swelling occurs via hydrolysis and sodium salt formation of residual carboxylic acid chloride groups on the trimesoyl linkages in the PA, followed by subsequent water absorption [40]. Despite the rigidity of fully aromatic polyamide structure, it has been shown that TMC/MPD-derived polyamides gain up to 28% in weight when exposed to water vapor [41,42]. The swelling behavior may be exacerbated in the presence of SDS.

Fig. 10 illustrates a proposed mechanism of hydrogen-bonding hydration of PA in the presence of SDS and water molecules. Both PA and SDS structures include electronegative atoms such as O and N in carbonyl, carboxylic and amine functional groups. The hydrogen-bonding acceptor and donor sites on these polar groups create many hydrogen bonding opportunities with water and other polar moieties. The PA layer consists of amide units that hydrogen bond with adjacent polyamide chains located in an amorphous domain. However, an equilibrium may exist in which water and SDS molecules break the inter-chain hydrogen bonds by forming intermolecular hydrogen bonds with these amide groups [43]. Thus, water and SDS can plasticize the amorphous portion of the polyamide network, causing the chain segments to slip and open the network structure [43–46]. Moreover, small cations and anions in water can stabilize and destabilize hydrogen-bonding through ionic hydration [47]. Therefore, as one of various stimuli-induced swelling behaviors, ion-specific swelling behavior observed for polymer gels in aqueous system cannot be neglected

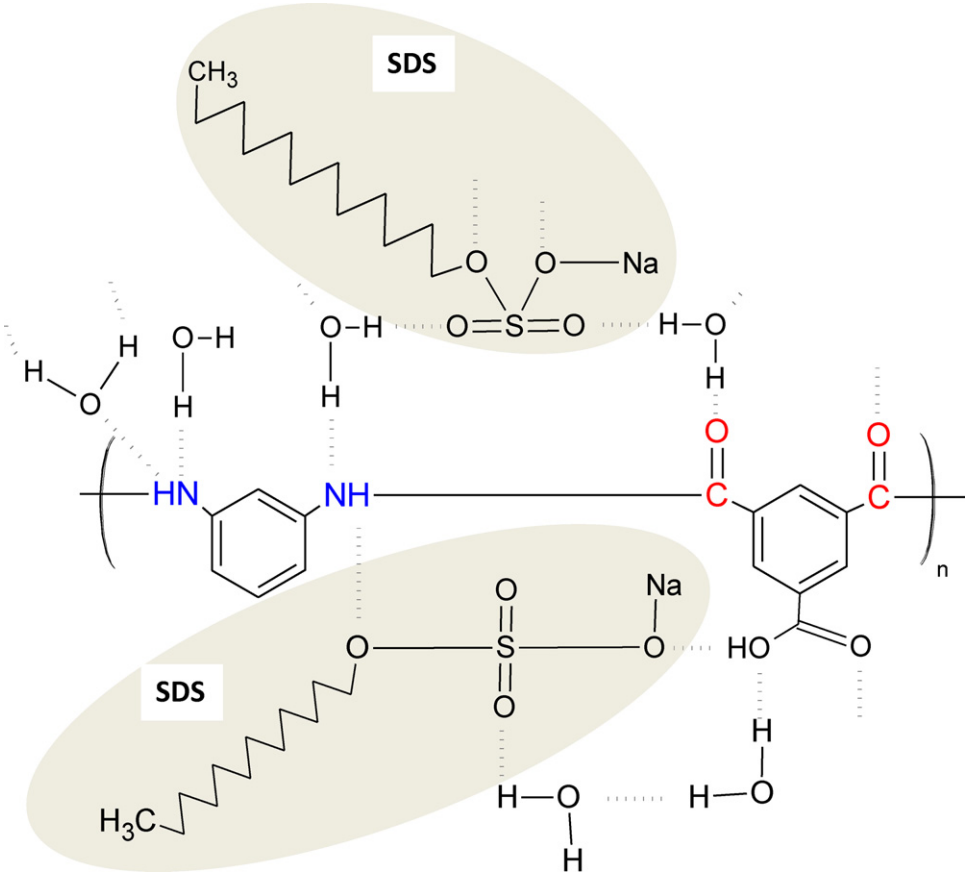

Fig. 10. Diagram of a possible arrangement of hydrogen-bonding hydration (dotted lines) of polyamide in the presence of sodium dodecyl sulfate (shaded areas).

[47]. In the circumstance of using SDS as a wetting agent, the presence of Na^+ and Cl^- may affect stabilization and destabilization of hydrogen-bonding hydration of polar polymers. As a consequence, the swelling of the polar polyamide skin layer may not be avoidable in the presence of SDS, NaCl, and water.

Moreover, SDS contacting with the back side of the PA layer may further contribute to plasticization. The PA layer is not a symmetric dense film and in fact has dual density gradients above and below its dense middle layer. The result is non-uniform distribution of crosslink density in the polyamide bulk [48,49]. The backside of the PA layer likely has lower density, and thus, enables deeper penetration of SDS. Therefore, plasticization effects that are exacerbated by ions may be enhanced. For example, the swelling mechanism may first occur at the edge of the membrane and gradually penetrate toward the dense inter-layer over time. Moreover, unlike traditional TFC membranes, the polyamide layer in these membranes has a less interfacial contact with the support membrane, and hence, the polyamide layer may be more susceptible to swelling than has traditionally been observed for TFC RO membranes.

4. Conclusions

In this study, a polyamide film was successfully polymerized over an electrospun nanofiber nonwoven support providing superior water flux and low salt flux for engineered osmosis applications. This support structure was chosen because of its superior porosity and pore interconnectivity which results in reduced internal concentration polarization. These novel membranes produced osmotic water fluxes two to five times higher than the commercial HTI-CTA osmotic membrane and compare favorably to other recently reported high flux osmotic membrane. While this departure from traditional polyamide composite membrane design shows immense promise as a next generation membrane platform for engineered osmosis, further exploration of polymer chemistry and fabrication procedures is needed to optimize performance. Next generation membranes such as these may also generate new insight into osmotic transport phenomenon and membranes tailored for specific engineered osmosis applications.

Acknowledgements

The authors acknowledge funding from the University of Connecticut Research Foundation and Center for Environmental Sciences and Engineering, Oasys Water®, The Department of Energy, and the UCLA California NanoSystems Institute. The authors graciously acknowledge Solvay Advanced Polymers for providing stock polymers for this work. Hydration Technologies Innovations provided the commercial cellulose acetate membrane for test comparisons and Freudenberg provided the polyester nonwoven. We also thank Dr. Joysurya Basu and Professor Barry Carter at the University of Connecticut for their assistance with the FIB SEM.

References

[1] R.L. McGinnis, M. Elimelech, Global challenges in energy and water supply: the promise of engineered osmosis, Environ. Sci. Technol. 42 (2008) 8625–8629.
[2] T.Y. Cath, A.E. Childress, M. Elimelech, Forward osmosis: principles, applications, and recent developments, J. Membr. Sci. 281 (2006) 70–87.
[3] J.R. McCutcheon, M. Elimelech, Influence of concentrative and dilutive internal concentration polarization on flux behavior in forward osmosis, J. Membr. Sci. 284 (2006) 237–247.
[4] G.T. Gray, J.R. McCutcheon, M. Elimelech, Internal concentration polarization in forward osmosis: role of membrane orientation, Desalination 197 (2006) 1–8.

[5] J.E. Cadotte, R.J. Petersen, Thin-film composite reverse-osmosis membranes: origin, development, and recent advances, Synth. Membr. 21 (1981) 305–326.
[6] J.E. Cadotte, Reverse osmosis membrane, US Patent 4,259,183 (1981).
[7] J.E. Cadotte, Interfacially synthesized reverse osmosis membrane, US Patent 4,277,344 (1981).
[8] R.J. Petersen, J.E. Cadotte, Thin film composite reverse osmosis membranes, in: M.C. Porter (Ed.), Handbook of Industrial Membrane Technology, Noyes Publications, NJ, 1988, pp. 307–348.
[9] M.L. Lind, A.K. Ghosh, A. Jawor, X. Huang, W. Hou, Y. Yang, E.M.V. Hoek, Influence of zeolite crystal size on zeolite-polyamide thin film nanocomposite membranes, Langmuir 25 (2009) 10139–10145.
[10] D. Mukherjee, A. Kulkarni, W.N. Gill, Chemical treatment for improved performance of reverse osmosis membranes, Desalination 104 (1996) 239–249.
[11] M. Hirose, H. Ito, Y. Kamiyama, Effect of skin layer surface structures on the flux behavior of RO membranes, J. Membr. Sci. 121 (1996) 209–215.
[12] I.J. Roh, S.Y. Park, J.J. Kim, C.K. Kim, Effects of the polyamide molecular structure on the performance of reverse osmosis membranes, J. Polym. Sci. Part B: Polym. Phys. 36 (1998) 1821–1830.
[13] A. Kulkarni, D. Mukherjee, W.N. Gill, Flux enhancement by hydrophilization of thin film composite reverse osmosis membranes, J. Membr. Sci. 114 (1996) 39–50.
[14] A.K. Ghosh, B.H. Jeong, X. Huang, E.M.V. Hoek, Impacts of reaction and curing conditions on polyamide composite reverse osmosis membrane properties, J. Membr. Sci. 311 (2008) 34–45.
[15] A.K. Ghosh, E.M.V. Hoek, Impacts of support membrane structure and chemistry on polyamide–polysulfone interfacial composite membranes, J. Membr. Sci. 336 (2009) 140–148.
[16] B.H. Jeong, E.M.V. Hoek, Y. Yan, A. Subramani, X. Huang, G. Hurwitz, A.K. Ghosh, A. Jawor, Interfacial polymerization of thin film nanocomposites: a new concept for reverse osmosis membranes, J. Membr. Sci. 294 (2007) 1–7.
[17] Y. Song, P. Sun, L.L. Henry, B. Sun, Mechanisms of structure and performance controlled thin film composite membrane formation via interfacial polymerization process, J. Membr. Sci. 251 (2005) 67–79.
[18] V. Freger, J. Gilron, S. Belfer, TFC polyamide membranes modified by grafting of hydrophilic polymers: an FT-IR/AFM/TEM study, J. Membr. Sci. 209 (2002) 283–292.
[19] S. Belfer, Y. Purinson, R. Fainshtein, Y. Radchenko, O. Kedem, Surface modification of commercial composite polyamide reverse osmosis membranes, J. Membr. Sci. 139 (1998) 175–181.
[20] H.I. Kim, S.S. Kim, Plasma treatment of polypropylene and polysulfone supports for thin film composite reverse osmosis membrane, J. Membr. Sci. 286 (2006) 193–201.
[21] A.P. Rao, S.V. Joshi, J.J. Trivedi, C.V. Devmurari, V.J. Shah, Structure-performance correlation of polyamide thin film composite membranes: effect of coating conditions on film formation, J. Membr. Sci. 221 (2003) 13–24.
[22] J.R. McCutcheon, M. Elimelech, Influence of membrane support layer hydrophobicity on water flux in osmotically driven membrane processes, J. Membr. Sci. 318 (2008) 166–458.
[23] K.L. Lee, R.W. Baker, H.K. Lonsdale, Membranes for power generation by pressure-retarded osmosis, J. Membr. Sci. 8 (1981) 141–171.
[24] H.K. Lonsdale, Recent advances in reverse osmosis membranes, Desalination 13 (1973) 317–332.
[25] J.R. McCutcheon, M. Elimelech, Modeling water flux in forward osmosis: implications for improved membrane design, AIChE J. 53 (2007) 1736–1744.
[26] C.H. Tan, H.Y. Ng, Modified models to predict flux behavior in forward osmosis in consideration of external and internal concentration polarizations, J. Membr. Sci. 324 (2008) 209–219.
[27] A. Achilli, T.Y. Cath, A.E. Childress, Power generation with pressure retarded osmosis: an experimental and theoretical investigation, J. Membr. Sci. 343 (2009) 42–52.
[28] A. Achilli, T.Y. Cath, A.E. Childress, Selection of inorganic-based draw solutions for forward osmosis applications, J. Membr. Sci. 364 (2010) 233–241.
[29] A. Tiraferri, N.Y. Yip, W.A. Phillip, J.D. Schiffman, M. Elimelech, Relating performance of thin-film composite forward osmosis membranes to support layer formation and structure, J. Membr. Sci. 367 (2011) 340–352.
[30] N.Y. Yip, A. Tiraferri, W.A. Phillip, J.D. Schiffman, M. Elimelech, High performance thin-film composite forward osmosis membrane, Environ. Sci. Technol. 44 (2010) 3812–3818.
[31] R. Wang, L. Shi, C.Y. Tang, S. Chou, C. Qiu, A.G. Fane, Characterization of novel forward osmosis hollow fiber membranes, J. Membr. Sci. 355 (2010) 158–167.
[32] J.T. Arena, B. McCloskey, B.D. Freeman, J.R. McCutcheon, Surface modification of thin film composite membrane support layers with polydopamine: enabling use of reverse osmosis membranes in pressure retarded osmosis, J. Membr. Sci. 375 (2011) 55–62.
[33] Z. Tang, C. Qiu, J.R. McCutcheon, K. Yoon, H. Ma, D. Fang, E. Lee, C. Kopp, B.S. Hsiao, B. Chu, Design and fabrication of electrospun polyethersulfone nanofibrous scaffold for high-flux nanofiltration membranes, J. Polym. Sci. Part B: Polym. Phys. 47 (2009) 2288–2300.
[34] P.H. Horward, Handbook of Environmental Fate and Exposure Data for Organic Chemicals, CRC Press, Boca Raton, FL, 1993.
[35] K. Yoon, B.S. Hsiao, B. Chu, Formation of functional polyethersulfone electrospun membrane for water purification by mixed solvent and oxidation processes, Polymer 50 (2009) 2893–2899.
[36] M.L. Lind, D.E. Suk, T.V. Nguyen, E.M.V. Hoek, Tailoring the structure of thin film nanocomposite membranes to achieve seawater RO membrane performance, Environ. Sci. Technol. 44 (2010) 8230–8235.
[37] Y. Liu, J.H. He, J.Y. Yu, H.M. Zeng, Controlling numbers and sizes of beads in electrospun nanofibers, Polym. Int. 57 (2008) 632–636.
[38] L.G. Wade, Reactions of aromatic compounds, in: Organic Chemistry, 5th ed., Pearson Education Inc., NJ, 2003, 747 pp.
[39] P.S. Singh, S.V. Joshi, J.J. Trivedi, C.V. Devmurari, A.P. Rao, P.K. Ghosh, Probing the structural variations of thin film composite RO membranes obtained by coating polyamide over polysulfone membranes of different pore dimensions, J. Membr. Sci. 278 (2006) 19–25.
[40] J.E. Cadotte, R.S. King, R.J. Majerle, R.J. Petersen, Interfacial synthesis in the preparation of reverse osmosis membrane, J. Macromol. Sci.-Chem. A15 (1981) 727–755.
[41] S.D. Arthur, Structure–property relationship in a thin film composite reverse osmosis membrane, J. Membr. Sci. 46 (1989) 243–260.
[42] V. Freger, Swelling and morphology of the skin layer of polyamide composite membranes: an atomic force microscopy study, Environ. Sci. Technol. 38 (2004) 3168–3175.
[43] H. Schott, Kinetics of swelling of polymers and their gels, J. Pharm. Sci. 81 (1992) 467–470.
[44] P.J. Flory, Principles of Polymer Chemistry, Cornell University Press, New York, 1953.
[45] N. Hirai, The Gel-Elasticity of High Polymers, Goto Laboratory, 1955, pp. 21–37.
[46] A.G. Tsuk, H.P. Gregor, Oleophilic ion-exchange polymers. II. Swelling of cross-linked networks with multiple hetero side chains, J. Am. Chem. Soc. 87 (1965) 5534–5537.
[47] H. Muta, M. Miwa, M. Satoh, Ion-specific swelling of hydrophilic polymer gels, Polymer 42 (2001) 6313–6316.
[48] V. Freger, Kinetics of film formation by interfacial polycondensation, Langmuir 21 (2005) 1884–1894.
[49] R. Nadler, S. Srebnik, Molecular simulation of polyamide synthesis by interfacial polymerization, J. Membr. Sci. 315 (2008) 100–105.
[50] S. Salgin, S. Takaç, T.H. Özdamar, Effect of ionic environments on the adsorption and diffusion characteristics of serine alkaline protease enzyme in polyethersulfone ultrafiltration membranes, J. Colloid Interface Sci. 299 (2006) 806–814.
[51] J.E. Mark, Polymer Data Handbook, Oxford University Press, 1999.